

A consistent analysis on QCD phase diagram and meson spectra in the improved soft-wall AdS/QCD

Zhen Fang,^{1,*} Yue-Liang Wu,^{2,3,†} and Lin Zhang^{2,4,‡}

¹*Department of Applied Physics, School of Physics and Electronics, Hunan University, Changsha 410082, China*

²*CAS Key Laboratory of Theoretical Physics, Institute of Theoretical Physics, Chinese Academy of Sciences, Beijing 100190, P. R. China*

³*International Centre for Theoretical Physics Asia-Pacific (ICTP-AP), University of Chinese Academy of Sciences, Beijing 100049, China*

⁴*School of Physical Sciences, University of Chinese Academy of Sciences, Beijing 100049, China*

(Dated: August 11, 2022)

Abstract

We present a consistent analysis on QCD phase diagram and meson spectra based on the improved soft-wall AdS/QCD. The equations of motion for the octet pseudoscalar, vector and axial-vector mesons with $2 + 1$ flavors are derived to calculate the octet meson spectra and relevant decay constants, by which the model parameters are determined. The chemical potential effects on chiral thermal transition are investigated, which enables us to obtain the QCD phase diagram in the $\mu - T$ plane. It is shown that the critical end point (CEP) linking the crossover transition with the first-order phase transition still exists and locates at $(\mu_B, T_c) \simeq (390 \text{ MeV}, 145 \text{ MeV})$. The crossover line and the location of CEP resulted from the model agree with both the lattice result and the experimental analysis from relativistic heavy-ion collisions. We find that the improved soft-wall AdS/QCD model can provide a consistent description for both the chiral phase diagram and the main properties of low-energy hadron physics in the $2 + 1$ flavor case.

Keywords: meson spectra, chiral transition, phase diagram, 2+1 flavor, AdS/QCD

* fangzhen@itp.ac.cn

† ylwu@itp.ac.cn

‡ zhanglin@itp.ac.cn

I. INTRODUCTION

As an important research area of quantum chromodynamics (QCD), there are still many puzzles on the phase transition of strongly interacting matters. Lattice simulations show evidence that the QCD matters exhibit a crossover transition with the increasing of temperature T at zero baryon number density [1–3]. It is generally believed that there is a critical end point (CEP) at some finite baryon density in the QCD phase diagram, and the crossover transition converts into the first-order one as the baryon chemical potential μ_B increases beyond the CEP [4–6]. The physics of the CEP and the search of it are crucial for our understanding of the QCD phase diagram, which have attracted extensive studies for decades, both theoretically and experimentally [7, 8]. However, no final conclusion has been reached on these matters. Lattice QCD as the first-principle calculation is hindered by the sign problem at finite chemical potential, though some tentative methods have been proposed to address this issue [9–12]. The QCD phase diagram with the properties of CEP were also studied in various effective models, see Ref. [7] for a review.

In this work, we continue the holographic QCD program aimed to study the low-energy physics of strong interaction in terms of the anti-de Sitter/conformal field theory (AdS/CFT) correspondence [13–15]. There have been large amounts of research works on the low-energy hadron physics and the thermal QCD phenomenons in this field over the past decade [16–63]. We focus on the realization of chiral phase transition in AdS/QCD, especially on the CEP-related properties of the QCD phase diagram, some of which have been considered from holography in recent years [64–78]. However, it is not that easy to give a consistent description for both the low-energy hadron properties and the QCD phase transitions in a single holographic framework.

In Ref. [79], we have proposed a simply improved soft-wall AdS/QCD model with reliable realization of linear confinement and spontaneous chiral symmetry breaking in the two-flavor case. The light meson spectra and the properties of chiral transition obtained from such a model conform well with the experimental or lattice results. We then generalized the improved soft-wall AdS/QCD model to the 2 + 1 flavor case, in which a 't Hooft determinate term of the bulk scalar field turns out to be crucial for the description of the quark-mass phase diagram [80]. The chemical potential effects on chiral transition have also been studied in the improved soft-wall AdS/QCD model. The QCD phase diagram in the $\mu - T$ plane was obtained, and the CEP linking the crossover transition with the first-order phase transition can be naturally produced [81]. Nevertheless, the model parameters used in the previous studies have been tuned by hand to realize the correct chiral transition behaviors, without any constraint from the low-energy hadron physics, e.g., the meson spectra with 2 + 1 flavors. Thus one may question if the same transition behaviors can be realized in the 2 + 1 flavor case when considering such low-energy hadron properties.

To check further the validity of the improved soft-wall AdS/QCD model and to give more realistic characterizations for the low-energy physics of QCD, we constrain the model parameters by the octet meson spectra and the related decay constants, then investigate the

relevant properties of chiral transition at finite baryon chemical potential. It will be shown that consistent results can be obtained for both the low-energy hadron properties and the chiral transitions, just as in the two-flavor case [79]. The CEP in the $\mu - T$ phase diagram still exists and locates at $(\mu_B, T_c) \simeq (390 \text{ MeV}, 145 \text{ MeV})$, which is consistent with the lattice or experimental indications.

The remaining part of the paper is organized as follows. In Sec. II, we outline the improved soft-wall AdS/QCD model with $2 + 1$ flavors. In Sec. III, we first derive the equation of motion (EOM) for the octet pseudoscalar, vector and axial-vector mesons, then fix the model parameters by calculating the octet meson spectra and the related decay constants. In Sec. IV, we investigate the chiral transition behaviors at finite μ_B , and calculate the $\mu - T$ phase diagram from the model. In Sec. V, we come to a brief summary of our work and conclude with some remarks.

II. THE IMPROVED SOFT-WALL ADS/QCD MODEL WITH $2 + 1$ FLAVORS

The improved soft-wall AdS/QCD model is built on the pure AdS₅ space in terms of the metric ansatz:

$$ds^2 = e^{2A(z)} (\eta_{\mu\nu} dx^\mu dx^\nu - dz^2) \quad (1)$$

with $\eta_{\mu\nu} = (+1, -1, -1, -1)$ and $A(z) = -\log \frac{z}{L}$, where the AdS radius will be taken as $L = 1$ for simplicity.

The bulk action of the improved soft-wall AdS/QCD model can be written as

$$S = \int d^5x \sqrt{g} e^{-\Phi(z)} \left[\text{Tr} \{ |DX|^2 - m_5^2(z) |X|^2 - \lambda |X|^4 - \frac{1}{4g_5^2} (F_L^2 + F_R^2) \} - \gamma \text{Re} \{ \det X \} \right], \quad (2)$$

where the covariant derivative of the bulk scalar field has the form of $D^M X = \partial^M X - iA_L^M X + iX A_R^M$, and the field strength $F_{L,R}^{MN} = \partial^M A_{L,R}^N - \partial^N A_{L,R}^M - i[A_{L,R}^M, A_{L,R}^N]$ with the chiral gauge field $A_{L,R}^M = A_{L,R}^{a,M} T^a = \frac{1}{2} A_{L,R}^{a,M} \lambda^a$, λ^a being the Gell-Mann matrices and $\text{Tr}(T^a T^b) = \frac{1}{2} \delta^{ab}$. The gauge coupling is determined as $g_5^2 = 12\pi^2/N_c$ with N_c being the color number [17]. The running mass of the scalar field takes the form: $m_5^2(z) = -3 - \mu_c^2 z^2$, the infrared (IR) asymptotics of which is empirically related to the low-energy hadron properties [79]. To give a better fitting for the ρ meson spectrum, we will use a modified dilaton profile in this work, i.e.,

$$\Phi(z) = \mu_g^2 z^2 \left(1 - e^{-\frac{1}{4}\mu_g^2 z^2} \right), \quad (3)$$

which has the IR asymptotic form $\Phi(z \rightarrow \infty) \sim z^2$ to reproduce the Regge spectra of the highly excited mesons. Here we shall note that the ultraviolet (UV) asymptotics of $\Phi(z)$ has very little effects on the properties of QCD phase diagram and other meson spectra in our model framework. A 't Hooft determinate term $\text{Re} \{ \det X \}$ has been added into the bulk action for the correct realization of chiral transition with $2 + 1$ flavors [56].

The vacuum expectation value (VEV) of the bulk scalar field has the form of

$$X_0 \equiv \langle X \rangle = \frac{1}{\sqrt{2}} \begin{pmatrix} \chi_u(z) & 0 & 0 \\ 0 & \chi_d(z) & 0 \\ 0 & 0 & \chi_s(z) \end{pmatrix} \quad (4)$$

with $\chi_u = \chi_d$ in the $2 + 1$ flavor case. The action of the scalar VEV X_0 can be obtained from the bulk action (2) as

$$S_\chi = \int d^5x \sqrt{g} e^{-\Phi(z)} [\text{Tr}\{\partial^z \langle X \rangle \partial_z \langle X \rangle - m_5^2(z) \langle X \rangle^2 - \lambda \langle X \rangle^4\} - \gamma \det \langle X \rangle], \quad (5)$$

from which the EOMs of $\chi_{u,s}$ can be derived as

$$\chi_u'' + (3A' - \Phi') \chi_u' - e^{2A} \left(m_5^2 \chi_u + \lambda \chi_u^3 + \frac{\gamma}{2\sqrt{2}} \chi_u \chi_s \right) = 0, \quad (6)$$

$$\chi_s'' + (3A' - \Phi') \chi_s' - e^{2A} \left(m_5^2 \chi_s + \lambda \chi_s^3 + \frac{\gamma}{2\sqrt{2}} \chi_u^2 \right) = 0. \quad (7)$$

Note that the EOMs of χ_u and χ_s are coupled with each other as a result of the 't Hooft determinate term of the bulk scalar field.

The UV asymptotic forms of the scalar VEV $\chi_{u,s}$ on the boundary $z = 0$ can be obtained from Eqs. (6) and (7) as

$$\chi_u(z \sim 0) = \frac{1}{\sqrt{2}} \left[m_u \zeta z - \frac{1}{4} m_u m_s \gamma \zeta^2 z^2 + \frac{\sigma_u}{\zeta} z^3 + \frac{1}{16} m_u \zeta \left(-\frac{1}{2} m_s^2 \gamma^2 \zeta^2 - \frac{1}{2} m_u^2 \gamma^2 \zeta^2 + 4 m_u^2 \zeta^2 \lambda - 8 \mu_c^2 \right) z^3 \ln z + \dots \right], \quad (8)$$

$$\chi_s(z \sim 0) = \frac{1}{\sqrt{2}} \left[m_s \zeta z - \frac{1}{4} m_u^2 \gamma \zeta^2 z^2 + \frac{\sigma_s}{\zeta} z^3 + \frac{1}{16} m_s \zeta \left(-m_u^2 \gamma^2 \zeta^2 + 4 m_s^2 \zeta^2 \lambda - 8 \mu_c^2 \right) z^3 \ln z + \dots \right], \quad (9)$$

where $m_{u,s}$ denotes the current quark mass and $\sigma_{u,s}$ the chiral condensate according to the AdS/CFT dictionary [17]. The normalization ζ is fixed by QCD as $\zeta = \frac{\sqrt{N_c}}{2\pi}$ [26]. The coefficient $\frac{1}{\sqrt{2}}$ is necessary to obtain the Gell-Mann–ŒOakes–ŒRenner (GOR) relation $m_\pi^2 f_\pi^2 = 2m_u \sigma_u$ for the two-flavor case [17]. The scalar VEV $\chi_{u,s}$ can be solved numerically from Eqs. (6) and (7) with the required IR asymptotics $\chi_{u,s}(z \rightarrow \infty) \sim z$ and the above UV boundary conditions.

III. OCTET MESON SPECTRA AND DECAY CONSTANTS

A. Input parameters

Now we consider the meson spectra with $2 + 1$ flavors and the relevant decay constants, which can be used to determine the model parameters μ_g , μ_c , γ and λ . The parameter μ_g can be fixed by the ρ meson spectrum, while γ and λ can be determined by the π meson spectrum and the pion decay constant. The parameter μ_c is strongly correlated with the critical chemical potential at the CEP and also affects the global fitting of the octet meson spectra. The physical quark masses $m_{u,s}$ are also slightly adjusted within the error range

$m_u(\text{MeV})$	$m_s(\text{MeV})$	$\mu_g(\text{MeV})$	$\mu_c(\text{MeV})$	λ	γ
3.24	98	480	877.8	130	-69.53

TABLE I. The input values of the model parameters in the numerical calculation. The quark masses $m_{u,s}$ are taken from Ref. [82].

of experiments in order to give the best fitting for the ground-state masses of the octet pseudoscalar mesons.

We first derive the EOMs of the octet pseudoscalar, vector and axial-vector mesons from the linearized bulk action (2), then we calculate the mass spectra of the octet mesons and fix the model parameters, the values of which are listed in Table I.

B. Octet pseudoscalar mesons

Following the usual procedure, the bulk scalar field X can be expressed as

$$X = \xi(X_0 + S^a T^a + S^0 T^0)\xi, \quad \xi = \exp(iT^a \pi^a) \quad (10)$$

with π^a being the pseudoscalar fields and S^a (S^0) being the $SU(3)$ octet (singlet) scalar fields. The scalar part will not be considered in our work. In the axial gauge $A_z = 0$, we decompose the axial gauge fields as $A_\mu^a = A_{\mu\perp}^a + \partial_\mu \phi^a$ in order to eliminate the cross terms of the pseudoscalar and axial-vector fields. With the Kaluza-Klein (KK) decomposition $\pi^a(x, z) = \sum_n \varphi_n(x) \pi_n^a(z)$, the EOM of the octet pseudoscalar mesons can be derived from the bulk action (2) as

$$\partial_z (e^{A-\Phi} \partial_z \phi_n^a) + 2g_5^2 e^{3A-\Phi} (M_A^2)_{ab} (\pi_n^b - \phi_n^b) = 0, \quad (11)$$

$$m_n^2 \partial_z \phi_n^a - 2g_5^2 e^{2A} (M_A^2)_{ab} \partial_z \pi_n^b = 0 \quad (12)$$

with

$$M_A^2 = \begin{pmatrix} \chi_u^2 \mathbf{1}_{3 \times 3} & 0 & 0 \\ 0 & \frac{1}{4}(\chi_u + \chi_s)^2 \mathbf{1}_{4 \times 4} & 0 \\ 0 & 0 & \frac{1}{3}(\chi_u^2 + 2\chi_s^2) \end{pmatrix}, \quad (13)$$

which can be solved numerically with the boundary conditions: $\pi_n^a(z \rightarrow 0) = \phi_n^a(z \rightarrow 0) = \partial_z \phi_n^a(z \rightarrow \infty) = 0$.

The calculated mass spectra of the octet pseudoscalar mesons are presented in Table II, where the experimental data are also shown for comparison. The data choosing is based on the suggested quark-model assignments for the observed light mesons [82]. We can see that the numerical results of the octet pseudoscalar meson spectra match with the experimental data quite well.

n	π exp. (MeV)	Model	K exp. (MeV)	Model	η exp. (MeV)	Model
0	139.57	139.57	493.677 ± 0.016	492.85	547.862 ± 0.017	585.19
1	1300 ± 100	1447	1460	1472	1476 ± 4	1485
2	1812 ± 12	1817	1874 ± 43	1836	1751 ± 15	1846

TABLE II. The calculated spectra of the octet pseudoscalar mesons compared with the experimental data, which are based on the suggested quark-model assignment for the observed light mesons [82].

C. Octet vector and axial-vector mesons

The chiral gauge fields are recombined into the vector field $V^M = \frac{1}{2}(A_L^M + A_R^M)$ and the axial-vector field $A^M = \frac{1}{2}(A_L^M - A_R^M)$. In the axial gauge $V_z = A_z = 0$ and with the KK decomposition, the EOMs for the octet vector and axial-vector mesons can be derived from the bulk action (2) as

$$\partial_z (e^{A-\Phi} \partial_z V_n^a) - 2g_5^2 e^{3A-\Phi} (M_V^2)_{ab} V_n^b + m_{V_n^a}^2 e^{A-\Phi} V_n^a = 0, \quad (14)$$

$$\partial_z (e^{A-\Phi} \partial_z A_n^a) - 2g_5^2 e^{3A-\Phi} (M_A^2)_{ab} A_n^b + m_{A_n^a}^2 e^{A-\Phi} A_n^a = 0, \quad (15)$$

where the matrix M_A^2 is given in (13) and M_V^2 takes the form:

$$M_V^2 = \begin{pmatrix} \mathbf{0}_{3 \times 3} & 0 & 0 \\ 0 & \frac{1}{4}(\chi_u - \chi_s)^2 \mathbf{1}_{4 \times 4} & 0 \\ 0 & 0 & 0 \end{pmatrix}. \quad (16)$$

Note that the octet axial-vector mesons are incorporated in the transverse part of the axial gauge fields $A_{\mu\perp}^a$.

Substituting the redefinition $V_n^a(z) = e^{\omega(z)/2} v_n^a(z)$ and $A_n^a(z) = e^{\omega(z)/2} a_n^a(z)$ with $\omega(z) = \Phi(z) - A(z)$ into the above Eqs. (14) and (15), and after some manipulations, we obtain the equivalent EOMs:

$$\partial_z^2 v_n^a + \left(\frac{1}{2} \omega'' - \frac{1}{4} \omega'^2 \right) v_n^a - 2g_5^2 e^{2A} (M_V^2)_{ab} v_n^b + m_{V_n^a}^2 v_n^a = 0, \quad (17)$$

$$\partial_z^2 a_n^a + \left(\frac{1}{2} \omega'' - \frac{1}{4} \omega'^2 \right) a_n^a - 2g_5^2 e^{2A} (M_A^2)_{ab} a_n^b + m_{A_n^a}^2 a_n^a = 0. \quad (18)$$

The mass spectra of the octet vector and axial-vector mesons can be obtained by solving the eigenvalue problem of Eqs. (17) and (18) with the following boundary conditions:

$$v_n^a(z \rightarrow 0) = 0, \quad \partial_z v_n^a(z \rightarrow \infty) = 0; \quad (19)$$

$$a_n^a(z \rightarrow 0) = 0, \quad \partial_z a_n^a(z \rightarrow \infty) = 0. \quad (20)$$

The numerical calculations for the spectra of vector and axial-vector mesons are given in Table III and IV, where we only present the ground-state data for the axial-vector octet

n	ρ exp. (MeV)	Model	K^* exp. (MeV)	Model	ϕ exp. (MeV)	Model
0	775.26 ± 0.25	775.1	891.76 ± 0.25	775.2	1019.461 ± 0.016	775.1
1	1465 ± 25	1335	1421 ± 9	1336	1680 ± 20	1335
2	1720 ± 20	1714	1718 ± 18	1714	2188 ± 10	1714

TABLE III. The model results of the octet vector meson spectra compared with the experimental data, which are based on the suggested quark-model assignment for the observed light mesons [82].

n	a_1 exp.(MeV)	Model	K_1 exp.(MeV)	Model	f_1 exp.(MeV)	Model
0	1230 ± 40	1115	1272 ± 7	1121	1426.4 ± 0.9	1122.8
1	—	1525	—	1528	—	1530
2	—	1854	—	1856	—	1857

TABLE IV. The model results of the octet axial-vector meson spectra compared with the experimental data, which are based on the suggested quark-model assignment for the observed light mesons [82].

in the light of the uncertainty of experiments [82]. We can see that the results obtained from the improved soft-wall AdS/QCD model are consistent with the experimental data except for the isosinglet states, i.e., the ϕ and f_1 mesons. For the vector octet, the matrix M_V^2 indicates that the isovector and isosinglet mesons have the same EOM, which leads to the same mass spectrum; while for the axial-vector octet, the terms of chiral symmetry breaking built in M_A^2 differ so little from each other that cannot distinguish the masses for the different axial-vector mesons. One might introduce high-order terms into the bulk action to improve the model results of the vector and axial-vector meson spectra without affecting the pseudoscalar part, e.g., $D_{[M}X D_{N]}X^\dagger F_L^{MN}$, $D_{[M}X^\dagger D_{N]}X F_R^{MN}$, $XX^\dagger F_L^{MN} F_{LMN}$, $X^\dagger X F_R^{MN} F_{RMN}$, $X F_R^{MN} X^\dagger F_{LMN}$. However, other model parameters will be introduced by this way, thus we will not consider in this work. One can refer to Ref. [30] for the effects of high-order terms on the octet meson spectra.

D. Decay constants of the pseudoscalar and (axial-)vector mesons

In view of the holographic recipe [17], the decay constants of the octet pseudoscalar mesons f_{π^a} can be extracted from the two-point correlation functions of the axial-vector currents as follows

$$f_{\pi^a}^2 = -\frac{1}{g_5^2} e^{A-\Phi} \partial_z A^a(0, z)|_{z \rightarrow 0}, \quad (21)$$

	$f_\pi(\text{MeV})$	$f_K(\text{MeV})$	$F_\rho^{1/2}(\text{MeV})$	$F_{a_1}^{1/2}(\text{MeV})$
Exp.	92.4	110	346.2 ± 1.4	433 ± 13
Model	92.4	100	307.1	350

TABLE V. The model results and the experimental values of the meson decay constants [17, 82].

where $A^a(0, z)$ is the solution of Eq. (15) in the case of $m_{A_n^a} = 0$ with the boundary conditions $A^a(0, 0) = 1$ and $\partial_z A^a(0, \infty) = 0$. Note that in the derivation of the decay constants f_{π^a} we have taken the limit $m_{\pi^a} \rightarrow 0$, which is only a good approximation for π meson [17].

The decay constants of ρ and a_1 mesons are given by

$$F_\rho^2 = \frac{1}{g_5^2} (e^{A-\Phi} \partial_z V_\rho(z)|_{z \rightarrow 0})^2, \quad (22)$$

$$F_{a_1}^2 = \frac{1}{g_5^2} (e^{A-\Phi} \partial_z A_{a_1}(z)|_{z \rightarrow 0})^2, \quad (23)$$

where $V_\rho(z)$ and $A_{a_1}(z)$ are the ground-state wave functions of ρ and a_1 mesons normalized by $\int dz e^{A-\Phi} V_\rho^2 = \int dz e^{A-\Phi} A_{a_1}^2 = 1$.

We show the model calculations for the decay constants f_π , f_K , F_ρ and F_{a_1} along with the experimental values in Table V, where f_π has been used as an input to determine the parameters γ and λ . We can see from Table V that the numerical results obtained from the model are consistent with the experimental results.

IV. CHIRAL TRANSITION AND QCD PHASE DIAGRAM

As the model parameters have been fixed by the octet meson spectra and the relevant decay constants, we now study the chemical potential effects on chiral transition in the improved soft-wall AdS/QCD model following Ref. [81]. To introduce the effects of temperature and chemical potential into the model, we use the AdS/Reissner-Nordstrom (AdS/RN) black hole solution as the bulk background with the metric ansatz:

$$ds^2 = e^{2A(z)} \left(f(z) dt^2 - dx^{i2} - \frac{dz^2}{f(z)} \right) \quad (24)$$

with

$$f(z) = 1 - (1 + Q^2) \left(\frac{z}{z_h} \right)^4 + Q^2 \left(\frac{z}{z_h} \right)^6, \quad (25)$$

where the charge Q of the black hole is related to the quark chemical potential μ_q by $Q = \mu_q z_h$ [64]. The baryon chemical potential is $\mu_B = 3\mu_q$. The Hawking temperature is given by

$$T = \frac{1}{4\pi} \left| \frac{df}{dz} \right|_{z_h} = \frac{1}{\pi z_h} \left(1 - \frac{Q^2}{2} \right), \quad 0 < Q < \sqrt{2}. \quad (26)$$

With the AdS/RN black-hole solution, the EOMs of the scalar VEV $\chi_{u,s}$ can be derived from the action (5) as

$$\chi_u'' + \left(\frac{f'}{f} + 3A' - \Phi' \right) \chi_u' - \frac{e^{2A}}{f} \left(m_5^2 \chi_u + \lambda \chi_u^3 + \frac{\gamma}{2\sqrt{2}} \chi_u \chi_s \right) = 0, \quad (27)$$

$$\chi_s'' + \left(\frac{f'}{f} + 3A' - \Phi' \right) \chi_s' - \frac{e^{2A}}{f} \left(m_5^2 \chi_s + \lambda \chi_s^3 + \frac{\gamma}{2\sqrt{2}} \chi_u^2 \right) = 0. \quad (28)$$

Under the prescription of AdS/CFT [17], the UV asymptotic forms $\chi_{u,s}(z \sim 0)$ can be obtained from the above EOMs with the chiral condensates $\sigma_{u,s}$ now depending on μ_B and T . The differences from those in Eqs. (8) and (9) are only incorporated in the high-order terms of z . At finite temperature, Eqs. (27) and (28) admit natural boundary conditions on the horizon z_h imposed by the regular property of χ_u and χ_s , i.e.,

$$f' \chi_u' - e^{2A} \left(m_5^2 \chi_u + \lambda \chi_u^3 + \frac{\gamma}{2\sqrt{2}} \chi_u \chi_s \right) \Big|_{z=z_h} = 0, \quad (29)$$

$$f' \chi_s' - e^{2A} \left(m_5^2 \chi_s + \lambda \chi_s^3 + \frac{\gamma}{2\sqrt{2}} \chi_u^2 \right) \Big|_{z=z_h} = 0. \quad (30)$$

As in Ref. [80], we can solve Eqs. (27) and (28) numerically with the given boundary conditions to obtain the profile of the scalar VEV $\chi_{u,s}$ and thus the chiral condensates $\sigma_{u,s}$ varying with μ_B and T . The chiral transitions of the condensates $\sigma_{u,s}$ with the temperature T at four different chemical potentials are shown in Fig. 1, where the distinction between the behaviors of $\sigma_u(T)$ and that of $\sigma_s(T)$ is due to the mass difference of m_u and m_s . We can see that the chiral transitions of $\sigma_{u,s}$ have a crossover behavior at small μ_B , and finally turn into first-order phase transitions with the increasing of μ_B . A second-order phase transition happens at $\mu_B \simeq 390$ MeV, which signifies the existence of CEP in the QCD phase diagram.

We calculate the chiral transition temperature T_c at each baryon chemical potential μ_B using the prescription given in Ref. [81]. The crossover transition temperature can be defined as the maximum of $|\frac{\partial \sigma_q}{\partial T}|$, while the critical temperature of the first-order phase transition is restricted to the range between the two inflections of the transition curve. The $\mu - T$ phase diagram obtained from the model is shown in Fig. 2, where the CEP linking the crossover transition at small μ_B with the first-order phase transition at larger μ_B has been highlighted by the red point with the location at $(\mu_B, T_c) \simeq (390 \text{ MeV}, 145 \text{ MeV})$. In Fig. 2, we also show the freeze-out data analyzed from the experiments of relativistic heavy-ion collisions and the crossover line obtained from the analytic continuation of lattice data with imaginary chemical potentials [83–88]. We can see that the crossover line and the location of CEP given by the improved soft-wall AdS/QCD model are consistent with the experimental analysis and the lattice result. However, the descent of T_c with the increasing of μ_B is too slow for the model prediction. The reason might be that the AdS/RN black-hole background adopted here is too simplified to produce more realistic chiral transitions, as in the case of deconfining phase transition, where one needs to solve the Einstein-Maxwell-Dilaton system with a fine-tuned dilaton potential to obtain the reasonable transition behaviors [45–48]. We

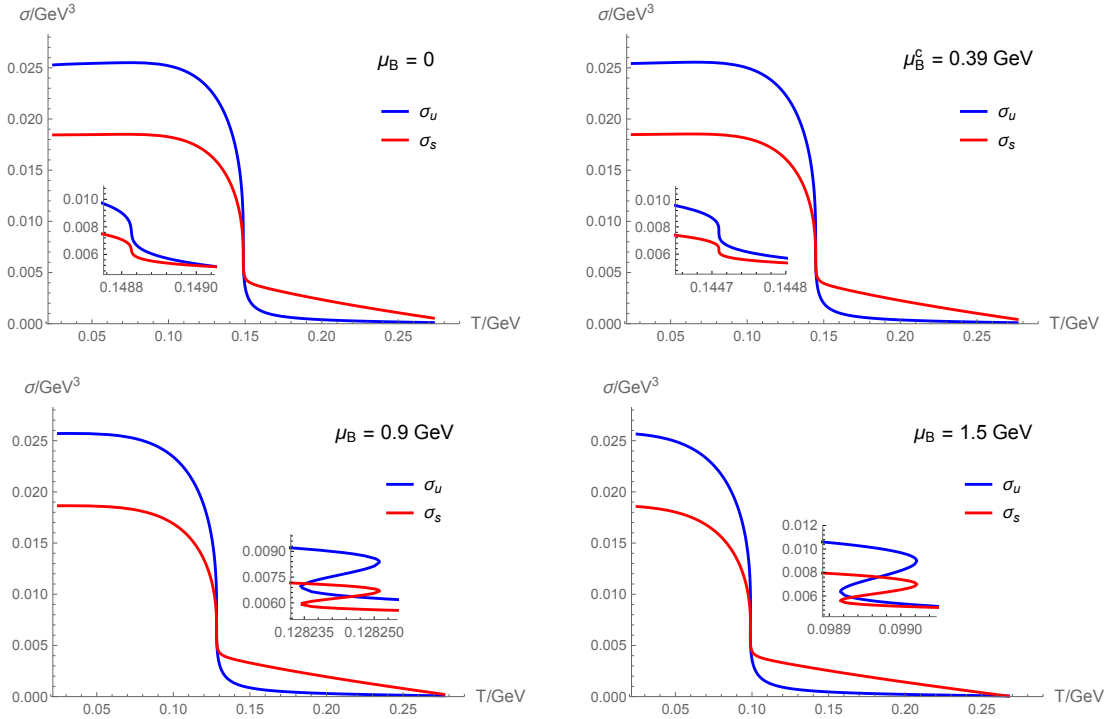


FIG. 1. The chiral transition behaviors of the condensates σ_u and σ_s with the temperature T at $\mu_B = 0, 0.39, 0.9, 1.5$ GeV.

also keep cautious on the reliability of our results obtained from the model at large enough μ_B .

V. CONCLUSION AND REMARKS

In this work, we have presented a further study on the improved soft-wall AdS/QCD model with $2 + 1$ flavors, which can reproduce the standard scenario of the quark-mass phase diagram [80]. A UV-modified dilaton field was adopted for a better fitting of the ρ meson spectrum. The EOMs for the octet pseudoscalar, vector and axial-vector mesons have been derived from this model framework. The octet meson spectra were calculated and compared with the experimental data. The model results for the octet pseudoscalar mesons agree well with the measurements. For the vector and axial-vector octets, the spectra of the isovector and isodoublet states are also consistent with experiments, yet the masses of the isosinglet states are much smaller than the experimental values. The reason for the mismatch can be seen obviously from the matrices M_V^2 and M_A^2 . The EOMs of the isosinglet mesons have the same form as those of the isovector mesons for the vector octet, while for the axial-vector octet the chiral symmetry breaking terms are too small to produce large mass difference. A possible way to address this issue is to consider high-order terms of the bulk action [30]. We also calculated the decay constants f_π , f_K , F_ρ and F_{a_1} , which are

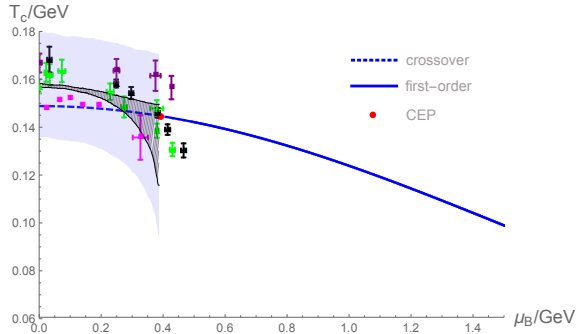


FIG. 2. The $\mu - T$ phase diagram obtained from the improved soft-wall AdS/QCD model. The colored points with error bars are freeze-out data analyzed from experiments. The black-triangle data are taken from Ref. [83, 84]. The green-triangle ones are taken from Ref. [85]. The purple squares are taken from Ref. [86]. The magenta squares are taken from Ref. [87]. The shaded black region shows the crossover line obtained from the lattice simulation at small μ_B , and the light blue band indicates the uncertainty width of the simulation [88].

comparable to the experimental results.

After fixing the model parameters by the octet meson spectra and the decay constants, we have studied the chemical potential effects on chiral transition and obtained the $\mu - T$ phase diagram, in which the CEP still exists and locates at $(\mu_B, T_c) \simeq (390 \text{ MeV}, 145 \text{ MeV})$. The crossover line and the location of CEP are consistent with the experimental analysis from relativistic heavy-ion collisions and the lattice results. However, the transition temperature T_c at large μ_B declines too slowly with the increasing of baryon chemical potential. In our work, the chemical potential effect is brought about by a fixed AdS/RN black hole, yet a more rational way is to consider the whole background system including the dilaton field. Nevertheless, as a preliminary attempt, we have shown that some main features of the low-energy hadron physics and the chiral phase diagram in the $\mu - T$ plane can be captured by a simply improved soft-wall AdS/QCD model in the holographic framework.

To obtain the expected chiral transition behaviors at large μ_B , it needs to take into account the effects of chemical potential and temperature by considering the Einstein-Maxwell-dilaton system, which also enables us to study the chiral and deconfining phase transitions in a single holographic framework. In addition, our current holographic QCD model might need further improvement to provide a better description for the octet meson spectra and other low-energy hadron properties. The back-reaction effect of the flavor part to the bulk background also deserves to be investigated in our model framework.

ACKNOWLEDGEMENTS

This work is partly supported by the National Science Foundation of China (NSFC) under Grants No. 11851302, No. 11851303, No. 11747601 and No. 11690022, and the Strategic Priority Research Program of the Chinese Academy of Sciences under Grant No. XDB23030100 as well as the CAS Center for Excellence in Particle Physics (CCEPP). It

is also supported by the Fundamental Research Funds for the Central Universities under Grant No. 531118010198.

-
- [1] Y. Aoki, G. Endrodi, Z. Fodor, S. D. Katz, and K. K. Szabo, *Nature* **443**, 675 (2006), arXiv:hep-lat/0611014 [hep-lat].
 - [2] A. Bazavov *et al.*, *Phys. Rev.* **D85**, 054503 (2012), arXiv:1111.1710 [hep-lat].
 - [3] T. Bhattacharya *et al.*, *Phys. Rev. Lett.* **113**, 082001 (2014), arXiv:1402.5175 [hep-lat].
 - [4] Z. Fodor and S. D. Katz, *JHEP* **03**, 014 (2002), arXiv:hep-lat/0106002 [hep-lat].
 - [5] Z. Fodor and S. D. Katz, *JHEP* **04**, 050 (2004), arXiv:hep-lat/0402006 [hep-lat].
 - [6] R. V. Gavai and S. Gupta, *Phys. Rev.* **D71**, 114014 (2005), arXiv:hep-lat/0412035 [hep-lat].
 - [7] M. A. Stephanov, *Proceedings, 24th International Symposium on Lattice Field Theory (Lattice 2006): Tucson, USA, July 23-28, 2006*, PoS **LAT2006**, 024 (2006), arXiv:hep-lat/0701002 [hep-lat].
 - [8] X. Luo and N. Xu, *Nucl. Sci. Tech.* **28**, 112 (2017), arXiv:1701.02105 [nucl-ex].
 - [9] Z. Fodor and S. D. Katz, *Phys. Lett.* **B534**, 87 (2002), arXiv:hep-lat/0104001 [hep-lat].
 - [10] C. R. Allton, S. Ejiri, S. J. Hands, O. Kaczmarek, F. Karsch, E. Laermann, C. Schmidt, and L. Scorzato, *Phys. Rev.* **D66**, 074507 (2002), arXiv:hep-lat/0204010 [hep-lat].
 - [11] P. de Forcrand and O. Philipsen, *Nucl. Phys.* **B642**, 290 (2002), arXiv:hep-lat/0205016 [hep-lat].
 - [12] H.-T. Ding, *Proceedings, 34th International Symposium on Lattice Field Theory (Lattice 2016): Southampton, UK, July 24-30, 2016*, PoS **LATTICE2016**, 022 (2017), arXiv:1702.00151 [hep-lat].
 - [13] J. M. Maldacena, *Int. J. Theor. Phys.* **38**, 1113 (1999), [Adv. Theor. Math. Phys.2,231(1998)], arXiv:hep-th/9711200 [hep-th].
 - [14] S. S. Gubser, I. R. Klebanov, and A. M. Polyakov, *Phys. Lett.* **B428**, 105 (1998), arXiv:hep-th/9802109 [hep-th].
 - [15] E. Witten, *Adv. Theor. Math. Phys.* **2**, 253 (1998), arXiv:hep-th/9802150 [hep-th].
 - [16] L. Da Rold and A. Pomarol, *Nucl. Phys.* **B721**, 79 (2005), arXiv:hep-ph/0501218 [hep-ph].
 - [17] J. Erlich, E. Katz, D. T. Son, and M. A. Stephanov, *Phys. Rev. Lett.* **95**, 261602 (2005), arXiv:hep-ph/0501128 [hep-ph].
 - [18] A. Karch, E. Katz, D. T. Son, and M. A. Stephanov, *Phys. Rev.* **D74**, 015005 (2006), arXiv:hep-ph/0602229 [hep-ph].
 - [19] G. F. de Teramond and S. J. Brodsky, *Phys. Rev. Lett.* **94**, 201601 (2005), arXiv:hep-th/0501022 [hep-th].
 - [20] S. J. Brodsky, G. F. de Teramond, H. G. Dosch, and J. Erlich, *Phys. Rept.* **584**, 1 (2015), arXiv:1407.8131 [hep-ph].
 - [21] J. Babington, J. Erdmenger, N. J. Evans, Z. Guralnik, and I. Kirsch, *Phys. Rev.* **D69**, 066007 (2004), arXiv:hep-th/0306018 [hep-th].
 - [22] M. Kruczenski, D. Mateos, R. C. Myers, and D. J. Winters, *JHEP* **05**, 041 (2004), arXiv:hep-th/0311270 [hep-th].

- [23] T. Sakai and S. Sugimoto, *Prog. Theor. Phys.* **113**, 843 (2005), arXiv:hep-th/0412141 [hep-th].
- [24] T. Sakai and S. Sugimoto, *Prog. Theor. Phys.* **114**, 1083 (2005), arXiv:hep-th/0507073 [hep-th].
- [25] C. Csaki and M. Reece, *JHEP* **05**, 062 (2007), arXiv:hep-ph/0608266 [hep-ph].
- [26] A. Cherman, T. D. Cohen, and E. S. Werbos, *Phys. Rev.* **C79**, 045203 (2009), arXiv:0804.1096 [hep-ph].
- [27] T. Gherghetta, J. I. Kapusta, and T. M. Kelley, *Phys. Rev.* **D79**, 076003 (2009), arXiv:0902.1998 [hep-ph].
- [28] T. M. Kelley, S. P. Bartz, and J. I. Kapusta, *Phys. Rev.* **D83**, 016002 (2011), arXiv:1009.3009 [hep-ph].
- [29] Y.-Q. Sui, Y.-L. Wu, Z.-F. Xie, and Y.-B. Yang, *Phys. Rev.* **D81**, 014024 (2010), arXiv:0909.3887 [hep-ph].
- [30] Y.-Q. Sui, Y.-L. Wu, and Y.-B. Yang, *Phys. Rev.* **D83**, 065030 (2011), arXiv:1012.3518 [hep-ph].
- [31] L.-X. Cui, Z. Fang, and Y.-L. Wu, *Eur. Phys. J.* **C76**, 22 (2016), arXiv:1310.6487 [hep-ph].
- [32] L.-X. Cui, Z. Fang, and Y.-L. Wu, *Chin. Phys.* **C40**, 063101 (2016), arXiv:1404.0761 [hep-ph].
- [33] D. Li, M. Huang, and Q.-S. Yan, *Eur. Phys. J.* **C73**, 2615 (2013), arXiv:1206.2824 [hep-th].
- [34] D. Li and M. Huang, *JHEP* **11**, 088 (2013), arXiv:1303.6929 [hep-ph].
- [35] G. Policastro, D. T. Son, and A. O. Starinets, *Phys. Rev. Lett.* **87**, 081601 (2001), arXiv:hep-th/0104066 [hep-th].
- [36] R.-G. Cai, Z.-Y. Nie, N. Ohta, and Y.-W. Sun, *Phys. Rev.* **D79**, 066004 (2009), arXiv:0901.1421 [hep-th].
- [37] R.-G. Cai, Z.-Y. Nie, and Y.-W. Sun, *Phys. Rev.* **D78**, 126007 (2008), arXiv:0811.1665 [hep-th].
- [38] S.-J. Sin and I. Zahed, *Phys. Lett.* **B608**, 265 (2005), arXiv:hep-th/0407215 [hep-th].
- [39] E. Shuryak, S.-J. Sin, and I. Zahed, *J. Korean Phys. Soc.* **50**, 384 (2007), arXiv:hep-th/0511199 [hep-th].
- [40] H. Nastase, (2005), arXiv:hep-th/0501068 [hep-th].
- [41] S. Nakamura and S.-J. Sin, *JHEP* **09**, 020 (2006), arXiv:hep-th/0607123 [hep-th].
- [42] S.-J. Sin, S. Nakamura, and S. P. Kim, *JHEP* **12**, 075 (2006), arXiv:hep-th/0610113 [hep-th].
- [43] R. A. Janik and R. B. Peschanski, *Phys. Rev.* **D73**, 045013 (2006), arXiv:hep-th/0512162 [hep-th].
- [44] C. P. Herzog, A. Karch, P. Kovtun, C. Kozcaz, and L. G. Yaffe, *JHEP* **07**, 013 (2006), arXiv:hep-th/0605158 [hep-th].
- [45] S. S. Gubser, A. Nellore, S. S. Pufu, and F. D. Rocha, *Phys. Rev. Lett.* **101**, 131601 (2008), arXiv:0804.1950 [hep-th].
- [46] S. S. Gubser and A. Nellore, *Phys. Rev.* **D78**, 086007 (2008), arXiv:0804.0434 [hep-th].
- [47] S. S. Gubser, S. S. Pufu, and F. D. Rocha, *JHEP* **08**, 085 (2008), arXiv:0806.0407 [hep-th].
- [48] O. DeWolfe, S. S. Gubser, and C. Rosen, *Phys. Rev.* **D83**, 086005 (2011), arXiv:1012.1864 [hep-th].
- [49] S. I. Finazzo and J. Noronha, *Phys. Rev.* **D90**, 115028 (2014), arXiv:1411.4330 [hep-th].
- [50] R. Yaresko and B. Kampfer, *Phys. Lett.* **B747**, 36 (2015), arXiv:1306.0214 [hep-ph].
- [51] D. Li, J. Liao, and M. Huang, *Phys. Rev.* **D89**, 126006 (2014), arXiv:1401.2035 [hep-ph].
- [52] D. Li, S. He, and M. Huang, *JHEP* **06**, 046 (2015), arXiv:1411.5332 [hep-ph].

- [53] Z. Fang, D. Li, and Y.-L. Wu, Phys. Lett. **B754**, 343 (2016), arXiv:1602.00379 [hep-ph].
- [54] Z. Fang, Phys. Rev. **D94**, 074017 (2016), arXiv:1607.06197 [hep-ph].
- [55] K. Chelabi, Z. Fang, M. Huang, D. Li, and Y.-L. Wu, Phys. Rev. **D93**, 101901 (2016), arXiv:1511.02721 [hep-ph].
- [56] K. Chelabi, Z. Fang, M. Huang, D. Li, and Y.-L. Wu, JHEP **04**, 036 (2016), arXiv:1512.06493 [hep-ph].
- [57] Z. Fang, S. He, and D. Li, Nucl. Phys. **B907**, 187 (2016), arXiv:1512.04062 [hep-ph].
- [58] N. Evans, C. Miller, and M. Scott, Phys. Rev. **D94**, 074034 (2016), arXiv:1604.06307 [hep-ph].
- [59] K. A. Mamo, Phys. Rev. **D94**, 041901 (2016), arXiv:1606.01598 [hep-th].
- [60] Z. Fang, Phys. Lett. **B758**, 1 (2016).
- [61] D. Dudal and S. Mahapatra, JHEP **04**, 031 (2017), arXiv:1612.06248 [hep-th].
- [62] D. Dudal and T. G. Mertens, Phys. Rev. **D97**, 054035 (2018), arXiv:1802.02805 [hep-th].
- [63] A. Ballon-Bayona, M. Ihl, J. P. Shock, and D. Zoakos, JHEP **10**, 038 (2017), arXiv:1706.05977 [hep-th].
- [64] P. Colangelo, F. Giannuzzi, S. Nicotri, and V. Tangorra, Eur. Phys. J. **C72**, 2096 (2012), arXiv:1112.4402 [hep-ph].
- [65] M. Jarvinen and E. Kiritsis, JHEP **03**, 002 (2012), arXiv:1112.1261 [hep-ph].
- [66] T. Alho, M. Jarvinen, K. Kajantie, E. Kiritsis, and K. Tuominen, JHEP **01**, 093 (2013), arXiv:1210.4516 [hep-ph].
- [67] T. Alho, M. Jarvinen, K. Kajantie, E. Kiritsis, C. Rosen, and K. Tuominen, JHEP **04**, 124 (2014), [Erratum: JHEP02,033(2015)], arXiv:1312.5199 [hep-ph].
- [68] M. Jarvinen, JHEP **07**, 033 (2015), arXiv:1501.07272 [hep-ph].
- [69] D. Li and M. Huang, JHEP **02**, 042 (2017), arXiv:1610.09814 [hep-ph].
- [70] S. P. Bartz and T. Jacobson, Phys. Rev. **D94**, 075022 (2016), arXiv:1607.05751 [hep-ph].
- [71] S. P. Bartz and T. Jacobson, Phys. Rev. **C97**, 044908 (2018), arXiv:1801.00358 [hep-ph].
- [72] R. Critelli, J. Noronha, J. Noronha-Hostler, I. Portillo, C. Ratti, and R. Rougemont, Phys. Rev. **D96**, 096026 (2017), arXiv:1706.00455 [nucl-th].
- [73] R. Critelli, R. Rougemont, and J. Noronha, JHEP **12**, 029 (2017), arXiv:1709.03131 [hep-th].
- [74] R. Rougemont, R. Critelli, and J. Noronha, Phys. Rev. **D98**, 034028 (2018), arXiv:1804.00189 [hep-ph].
- [75] R. Critelli, R. Rougemont, and J. Noronha, (2018), arXiv:1805.00882 [hep-th].
- [76] Z. Li, Y. Chen, D. Li, and M. Huang, Chin. Phys. **C42**, 013103 (2018), arXiv:1706.02238 [hep-ph].
- [77] X. Chen, D. Li, and M. Huang, (2018), arXiv:1810.02136 [hep-ph].
- [78] J. Chen, S. He, M. Huang, and D. Li, JHEP **01**, 165 (2019), arXiv:1810.07019 [hep-ph].
- [79] Z. Fang, Y.-L. Wu, and L. Zhang, Phys. Lett. **B762**, 86 (2016), arXiv:1604.02571 [hep-ph].
- [80] Z. Fang, Y.-L. Wu, and L. Zhang, Phys. Rev. **D98**, 114003 (2018), arXiv:1805.05019 [hep-ph].
- [81] Z. Fang, Y.-L. Wu, and L. Zhang, Phys. Rev. **D99**, 034028 (2019), arXiv:1810.12525 [hep-ph].
- [82] M. Tanabashi *et al.* (Particle Data Group), Phys. Rev. **D98**, 030001 (2018).
- [83] F. Becattini, J. Manninen, and M. Gazdzicki, Phys. Rev. **C73**, 044905 (2006), arXiv:hep-ph/0511092 [hep-ph].
- [84] J. Cleymans, B. Kampfer, M. Kaneta, S. Wheaton, and N. Xu, Phys. Rev. **C71**, 054901 (2005), arXiv:hep-ph/0409071 [hep-ph].

- [85] A. Andronic, P. Braun-Munzinger, and J. Stachel, Phys. Lett. **B673**, 142 (2009), [Erratum: Phys. Lett.B678,516(2009)], arXiv:0812.1186 [nucl-th].
- [86] F. Becattini, M. Bleicher, T. Kollegger, T. Schuster, J. Steinheimer, and R. Stock, Phys. Rev. Lett. **111**, 082302 (2013), arXiv:1212.2431 [nucl-th].
- [87] P. Alba, W. Alberico, R. Bellwied, M. Bluhm, V. Mantovani Sarti, M. Nahrgang, and C. Ratti, Phys. Lett. **B738**, 305 (2014), arXiv:1403.4903 [hep-ph].
- [88] R. Bellwied, S. Borsanyi, Z. Fodor, J. GÅijnter, S. D. Katz, C. Ratti, and K. K. Szabo, Phys. Lett. **B751**, 559 (2015), arXiv:1507.07510 [hep-lat].

